Biophysical Journal, Volume *121*

Supplemental information

Characterizing fenestration size in sodium channel subtypes and their accessibility to inhibitors

Elaine Tao and Ben Corry

Table S1 | Summary of recently published cryo-EM eukaryotic sodium channel structures.

*Structures simulated in bold. *5X0M was not part of the main study (addendum to the discussion).*

PDB ID	Subtype	Citation	Resolution (Å)	Voltage sensor state	Pore gate state	Inactivation Motif State	Co-resolved ligands/ peptide toxins	Auxilary subunits
7DTD	Nav1.1 (human)	(Pan et al., 2021)	3.3	All activated	Partially open by detergent	Bound	-	β4
6J8E	Nav1.2 (human)	(Pan et al., 2019)	3.0	All activated	Partially open by detergent	Bound	μ-conotoxin KIIIA (blocking SF)	β2
6AGF	Nav1.4 (human)	(Pan et al., 2018)	3.2	All activated	Partially open by detergent	Bound	-	β1
6UZ0	Nav1.5 (rat)	(Jiang et al., 2020)	3.5	All activated	Partially open by detergent	Bound	Flecainide (in central cavity/ DII-III)	-
6UZ3	Nav1.5 (rat)		3.5	All activated	Partially open by detergent	Bound	-	-
6LQA	Nav1.5 (human)	(Li et al., 2021a)	3.3	All activated	Tightly closed	Bound	Quinidine (in central cavity)	-
7DTC	Nav1.5-E1784K (human)	(Li et al., 2021b)	3.3	All activated	Closed	Bound	-	-
7K18	Nav1.5 (rat)	(Jiang et al., 2021b)	3.3	All activated, VS-DIV partially activated	Partially open (shift in S6 helices)	Bound (less stable)	LqhIII toxin (bound to VS-DIV)	-
7FBS	Nav1.5-QQQ (rat)	(Jiang et al., 2021a)	3.3	All activated	Open (allows conduction)	Unbound (IFM mutated to QQQ)	Propafenone (in central cavity, near selectivity filter)	-
6J8G	Nav1.7 (human)	(Shen et al., 2019)	3.2	Only VS-DII inactivated	Closed	Bound	Tetrodotoxin (blocking SF), protoxin-II (bound to VS-DII)	β1, β2
6J8H	Nav1.7 (human)		3.2	Only VS-DII inactivated	Closed	Bound	Saxitoxin (blocking SF), huwentoxin-II (bound to VS-DII)	β1, β2
6J8I	Nav1.7 (human)		3.2	Only VS-DII inactivated	Closed	Bound	-	β1, β2
6J8J	Nav1.7 (human)		3.2	Only VS-DII inactivated	Closed	Bound	-	β1, β2
5X0M*	NavPas (cockroach)	(Shen et al., 2017)	3.8	Varying degrees of activation	Tightly closed	No IFM motif (DIII-IV linker sequestered by CTD	-	-

Table S2 | System sizes for Nav subtype structures

SYSTEM	*BOX DIMENSIONS (x, y, z)*	*TOTAL ATOMS*
Nav1.1	164, 162, 143	336069
Nav1.2	161, 161, 129	295219
Nav1.4	158, 158, 128	280711
Nav1.5	162, 161, 140	323456
Nav1.5r	162, 160, 135	310798
Nav1.7	157, 157, 127	277117
NavPas	166, 165, 160	392809

Table S3 | MD Parameters for pre-equilibration setup and production steps using AMBER.

NPT (constant particle number, pressure and temperature); NVT (constant particle number, volume and temperature);aniso (anisotropic); CYC (cycles); γ_ln (collision frequency); τ_p (relaxation time); CA (protein α-Carbon atoms).

	STEP	**ENS**	**TIME / CYC**	**TEMPERATURE**			**PRESSURE**			**RESTRAINTS (kcal.mol^{-1}.Å^{-2})**
				K	Thermostat	γ_ln (ps^{-1})	atm	Barostat	τ_p (ps)	
CPU	***Minimisation1***	NVT	1000cyc	-	-	-	-	-	-	25 (all atoms except water and hydrogen)
	Minimisation2	NVT	1000cyc	-	-	-	-	-	-	5 (CA)
	Minimisation3	NVT	1000cyc	-	-	-	-	-	-	-
	Heat	NPT - aniso	0.25ns	0-310	Langevin	5	-	Berendsen	1	5 (CA)
	Hold1	NPT - aniso	0.5ns	310	Langevin	5	1	Monte Carlo	1	5 (CA)
GPU	***Hold2***	NPT - aniso	9 x 0.5 = 4.5ns	310	Langevin	5	1	Monte Carlo	1	5 (CA)
	Restraint Reduction	NPT - aniso	12 x 2 = 24ns	310	Langevin	5	1	Monte Carlo	1	4, 3, 2, 1, 0.8, 0.6, 0.4, 0.2, 0.1, 0.05, 0.02, 0.01 (CA)
	Production (Equilibrium MD)	NPT - aniso	500ns	310	Langevin	5	1	Monte Carlo	1	-

Table S4 | Parameters used for CAVER tunnel identification.

starting_point_residue	*midpoint residue of DIS6**
starting_point_residue	*midpoint residue of DIIS6**
starting_point_residue	*midpoint residue of DIIIS6**
starting_point_residue	*midpoint residue of DIVS6**
probe_radius	0.8
shell_radius	15
shell_depth	15
number_of_approximating_balls	12
bottleneck_contact_distance	3
clustering	average_link
weighting_coefficient	1
clustering_threshold	10
do_approximate_clustering	yes
cluster_by_hierarchical_clustering	20000
max_training_clusters	14
generate_unclassified_cluster	no
murtagh_matrix_size	*between 9000 to 12000*

**geometric centre of the four starting_point_residues used to calculate the starting point for tunnel calculations (located roughly at the centre of the pore cavity)*

Table S5 | Summary of bottleneck radii statistics.

Average, maximum and standard deviation (StDev) calculated for each subtype and fenestration, combining across all three replicates.

SUBTYPE (PDB)	FENESTRATION	BOTTLENECK RADIUS (Å)			
		Starting Structure	Overall Average	Maximum	StDev
NAV1.1 (7DTD)	DI-II	1.88	1.97	2.93	0.31
	DII-III	2.10	1.50	2.59	0.31
	DIII-IV	2.43	2.05	2.85	0.25
	DI-IV	1.95	1.42	2.75	0.56
NAV1.2 (6J8E)	DI-II	2.26	1.98	2.91	0.30
	DII-III	2.24	1.77	2.72	0.35
	DIII-IV	2.59	2.02	2.78	0.24
	DI-IV	1.92	1.65	2.82	0.56
NAV1.4 (6AGF)	DI-II	2.25	1.95	3.27	0.41
	DII-III	2.46	1.73	2.70	0.40
	DIII-IV	2.54	1.57	2.77	0.49
	DI-IV	1.92	1.00	2.48	0.31
NAV1.5 - HUMAN (6UZ0 - HOMOLOGY)	DI-II	2.19	2.25	3.35	0.25
	DII-III	1.64	1.61	2.84	0.48
	DIII-IV	2.15	1.84	2.71	0.35
	DI-IV	1.82	0.92	2.35	0.14
NAV1.5 -RAT (6UZ0)	DI-II	2.40	1.99	2.89	0.28
	DII-III	1.80	1.65	2.70	0.43
	DIII-IV	2.02	1.85	2.72	0.33
	DI-IV	1.03	1.04	2.21	0.20
NAV1.7 (6J8G)	DI-II	2.19	2.09	3.01	0.33
	DII-III	2.05	1.69	2.70	0.31
	DIII-IV	2.58	2.02	2.76	0.24
	DI-IV	0.91	1.01	2.40	0.29
NAVPAS (5X0M)	DI-II	<0.8	0.87	1.62	0.12
	DII-III	<0.8	0.87	1.66	0.13
	DIII-IV	1.34	1.45	2.76	0.40
	DI-IV	0.82	0.93	1.71	0.14

Table S6 | SCN1A (Nav1.1) disease-related mutations identified to be in fenestration bottleneck residues.

Mutations were extracted from UNIPROT website (Bateman et al., 2020)
DS; Dravet's syndrome; GEFS+2: Generalized epilepsy with febrile seizures plus 2; ICEGTC: Intractable childhood epilepsy with generalized tonic-clonic seizures.

RESIDUE	MUTATION	CONDITION	FENESTRATION
379	M → R	DS	DI-II
976	M → I	DS, GEFS+2	DI-II
983	V → A	ICEGTC	DII-III
986	L → F	DS	DII-III
986	L → P	DS	DII-III
1472	F → S	DS	DII-III
1355	L → P	DS	DIII-IV
1358	W → R	DS	DIII-IV
1358	W → S	DS	DIII-IV
1426	L → R	DS	DIII-IV
1429	A → D	ICEGTC	DIII-IV
1429	Deletion	DS	DIII-IV
1475	L → S	DS	DIII-IV
1770	I → F	DS	DIII-IV
1770	I → N	DS	DIII-IV
1770	I → T	DS	DIII-IV
1771	I → F	DS	DIII-IV
1771	I → N	DS	DIII-IV
1677	L → F	DS	DI-IV
1721	T → R	DS	DI-IV
1780	M → T	DS	DI-IV
1781	Y → C	DS, ICEGTC	DI-IV
1781	Y → H	DS	DI-IV

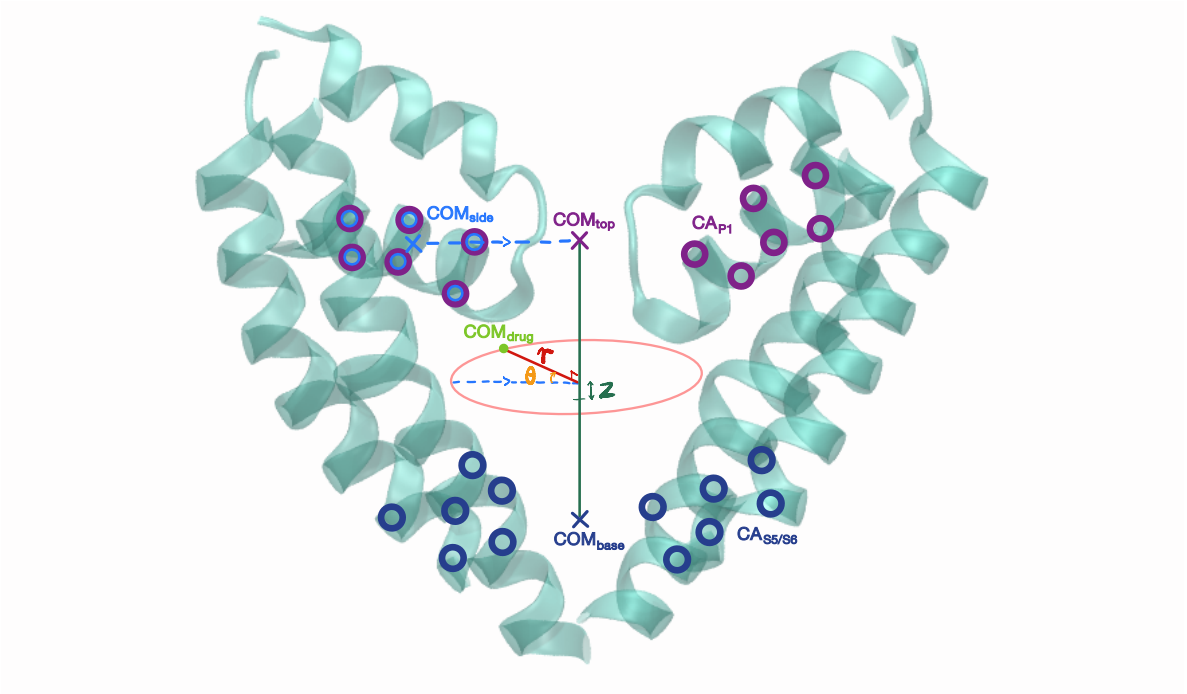

Figure S1 | Geometrically defining the collective variables for lidocaine position relative to the protein.

The three-dimensional coordinates for the centre of mass of lidocaine (COM_{drug}) was defined relative to the sodium channel structure, using six carbon-alpha (CA) atoms in P1 of each domain and six CA atoms at the S5-S6 helices of each domain to define the centre axis; and the same six CA atoms in P1 of only DI and DII to define the angular reference point. Only two opposite domains are shown here. z is the projected position of COM_{drug} along the axis from the midpoint; r is the perpendicular distance of COM_{drug} from the axis; and θ is the angle between the COM_{drug} vector and the reference.

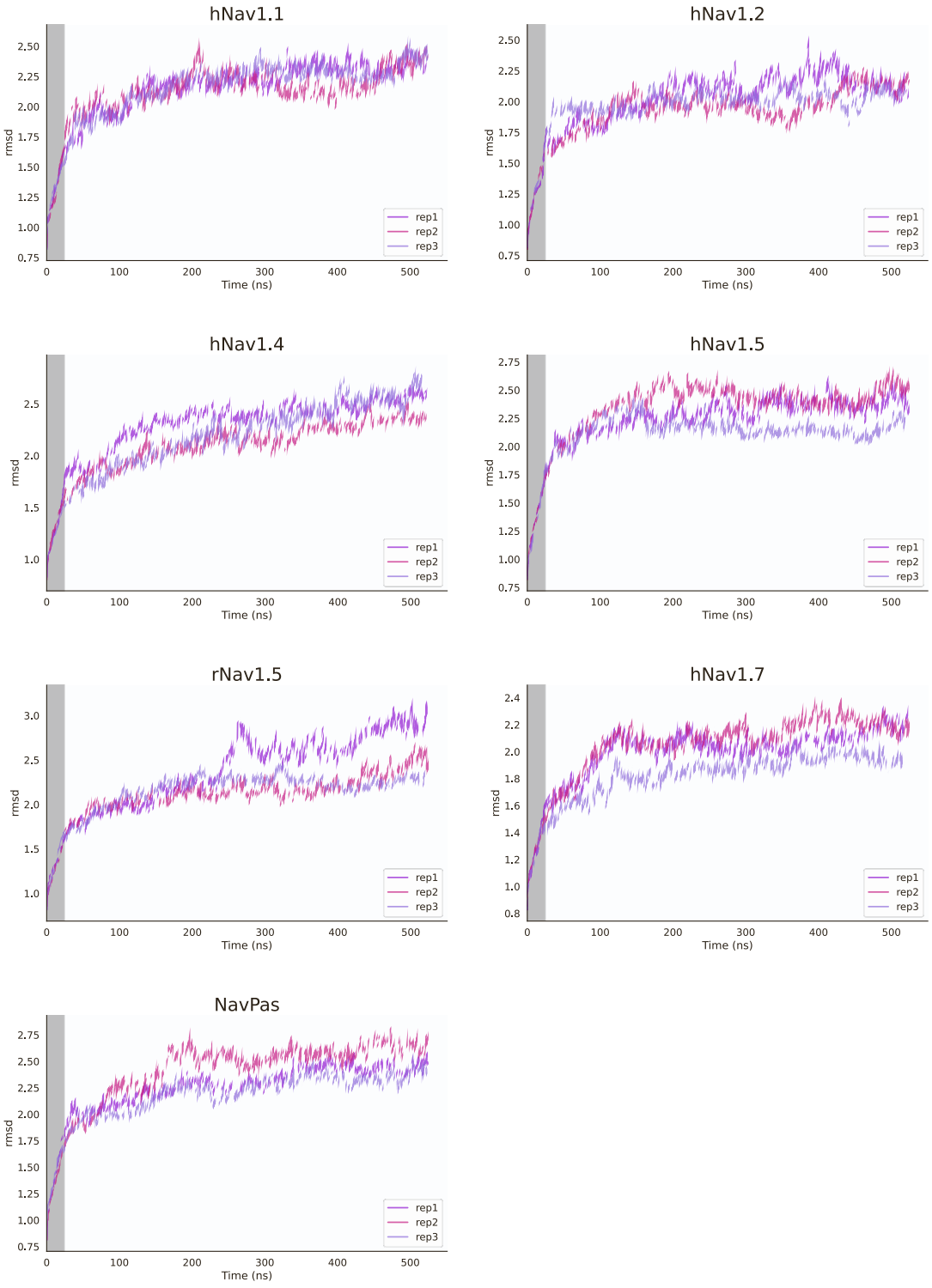

Figure S2 | RMSD of the pore module for three replicates of all seven simulation systems.

First 24ns of reducing restraints (pre-equilibration step) indicated by grey region, followed by 500ns of equilibrium MD production runs.

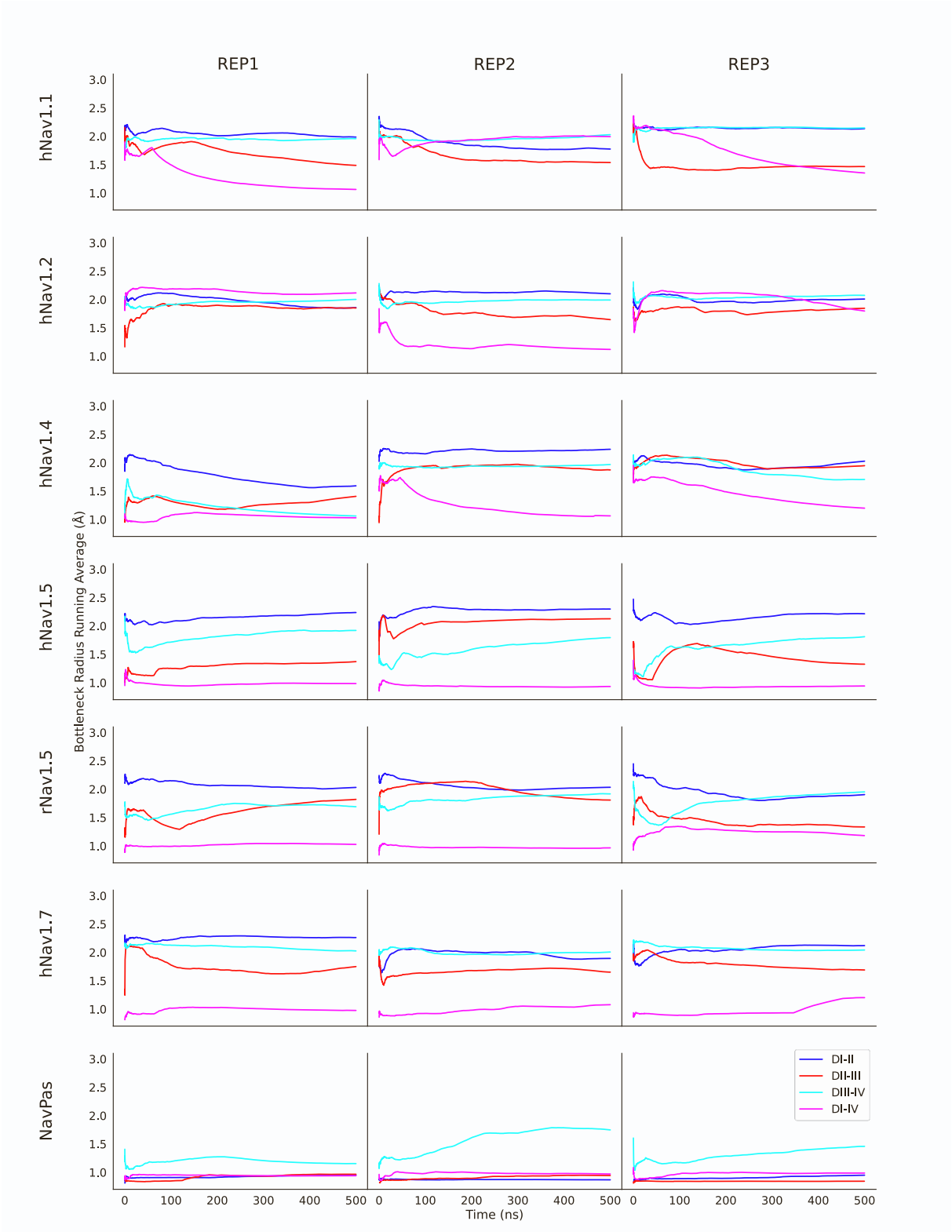

Figure S3 | Running average of bottleneck radius for each fenestration of each equilibrium simulations.

Fenestration bottleneck radius averages in all the replicates flatten out over the course of the 500 ns runs; however, the three replicates do not appear to converge to the same values.

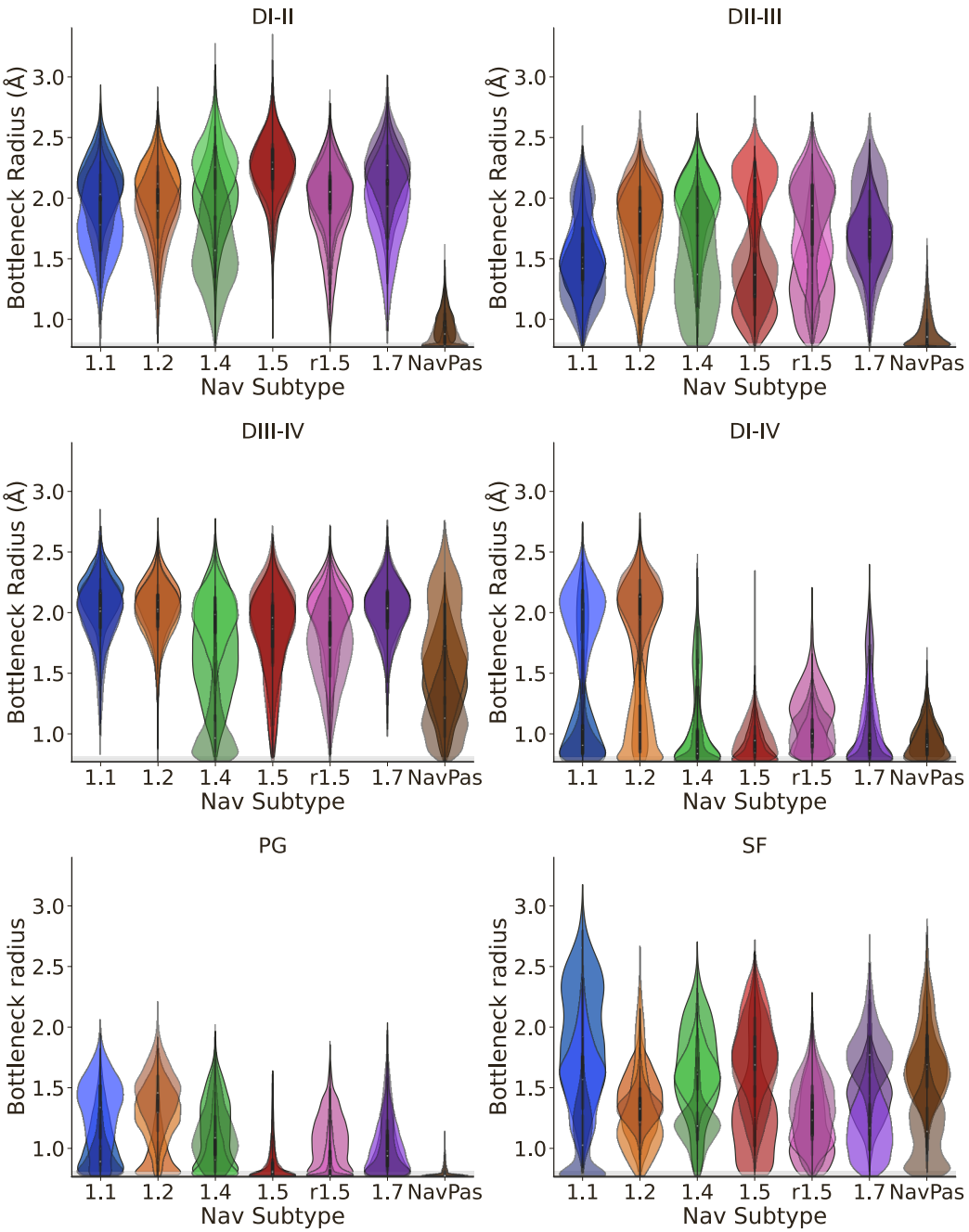

Figure S4 | Bottleneck radius distributions across Nav subtypes distinguishing between the three separate replicates.

Extended version of Figure 4, showing the difference in bottleneck radius distribution across the different fenestrations, as well as variability in pore gate (PG) and selectivity filter (SF) bottleneck radius distributions.

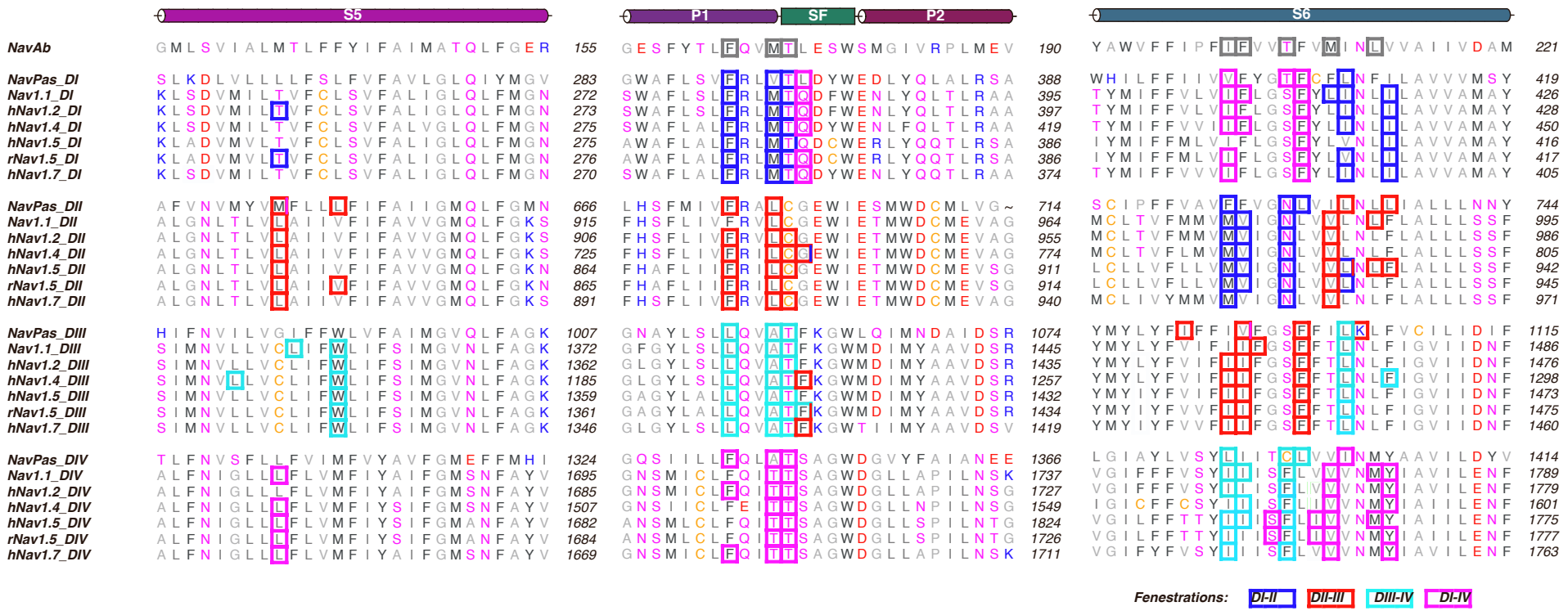

Figure S5 | Sequence Alignment of Pore Modules of Sodium Channel Subtypes by Fenestration

Each domain is aligned to the NavAb sequence, showing that the transmembrane portions of the pore module (i.e., S5, P1, SF, P2 and S6) for each domain is highly conserved between subtypes but less so between the four domains. Extracellular/turret loops were omitted for conciseness. Top identified bottleneck residues for each fenestration, which are boxed with different colours – DI-II (blue), DII-III (red), DIII-IV (cyan), DI-IV (magenta), are also fairly consistent across subtypes. Bottleneck residues identified in NavAb from a previous study (Kaczmarski and Corry, 2014) boxed in grey.

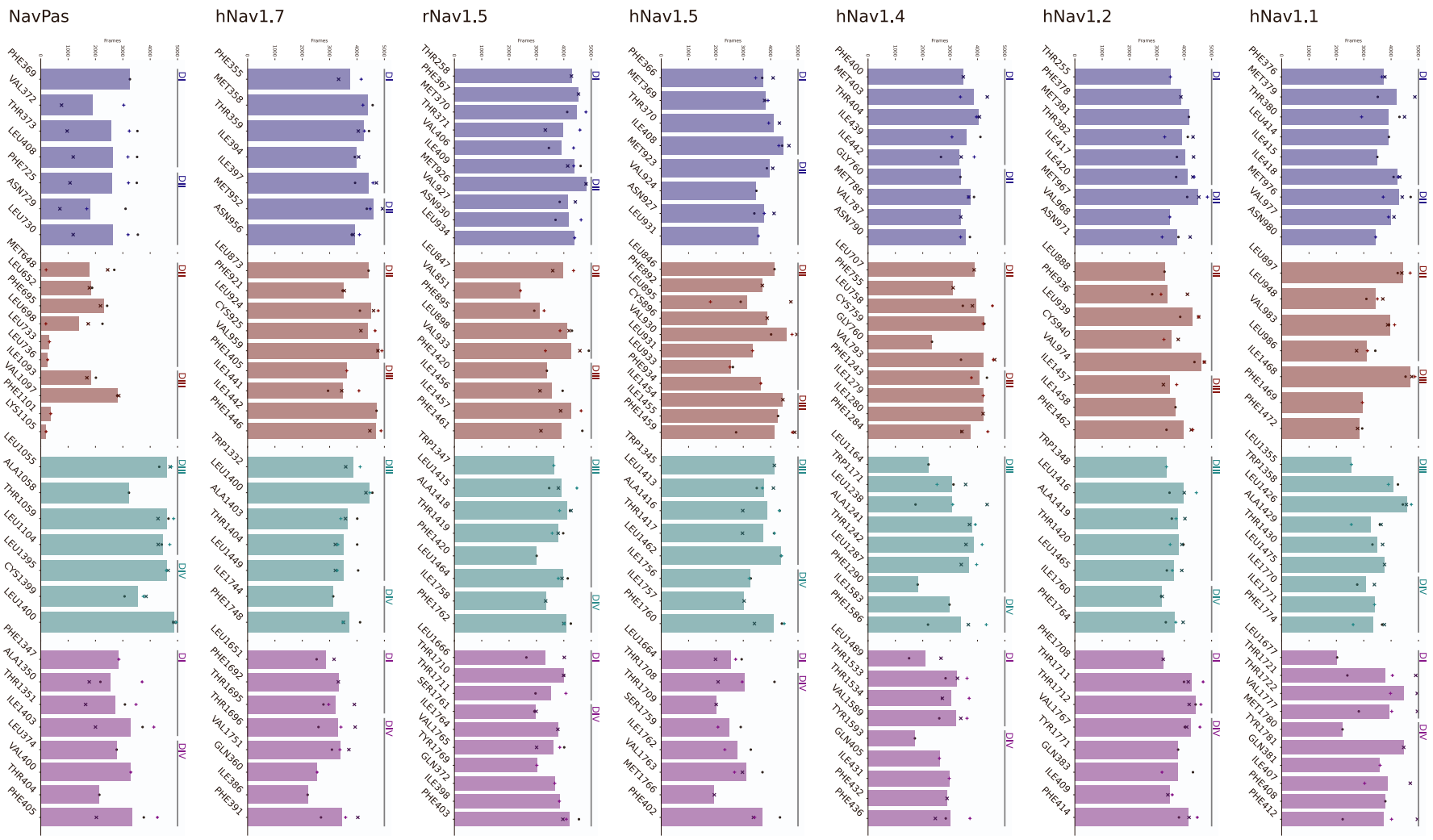

Figure S6 | Top bottleneck residues in each fenestration.

Top six bottleneck residues were identified in each of the three replicates, showing the average number of frames the specific residue was identified across all three replicates; number of frames for individual replicates depicted by · (Replicate 1), × (Replicate 2), and + (Replicate 3). Coloured according to fenestration each bottleneck residue is found in - DI-II (blue), DII-III (red), DIII-IV (cyan), DI-IV (magenta).

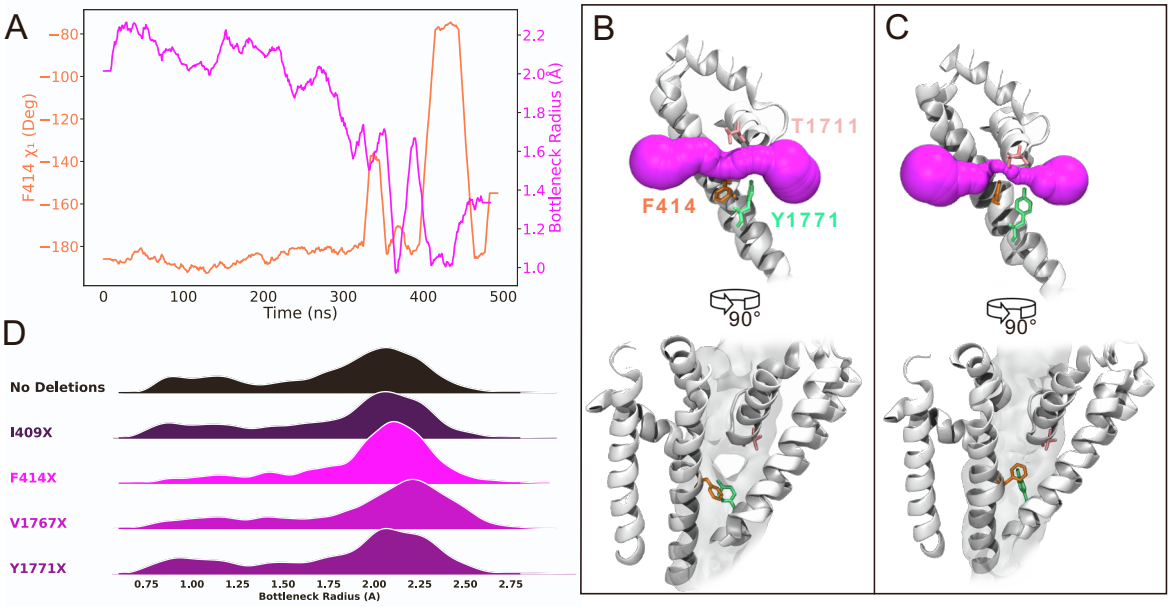

Figure S7 | S6 phenylalanine residue (F414) at position 15 is responsible for gating fenestration DI-IV.

F414 χ1 dihedral angle is correlated with DI-IV bottleneck radius in hNav1.2 (A). Representative snapshots for F414 being in the 'down' configuration resulting in a wide fenestration bottleneck radius (B); compared to F414 being in the 'up' configuration resulting in a narrowed fenestration bottleneck radius (C). Bottleneck radius distributions after individual sidechain deletions of bottleneck residues in DI-IV of on replicate of hNav1.2 (D) demonstrates that deletion of the F414 aromatic sidechain reduced occurrence of the narrowed fenestration bottleneck radius (however, the effects are less profound compared to DII-III of Nav1.5 shown in Figure 5).

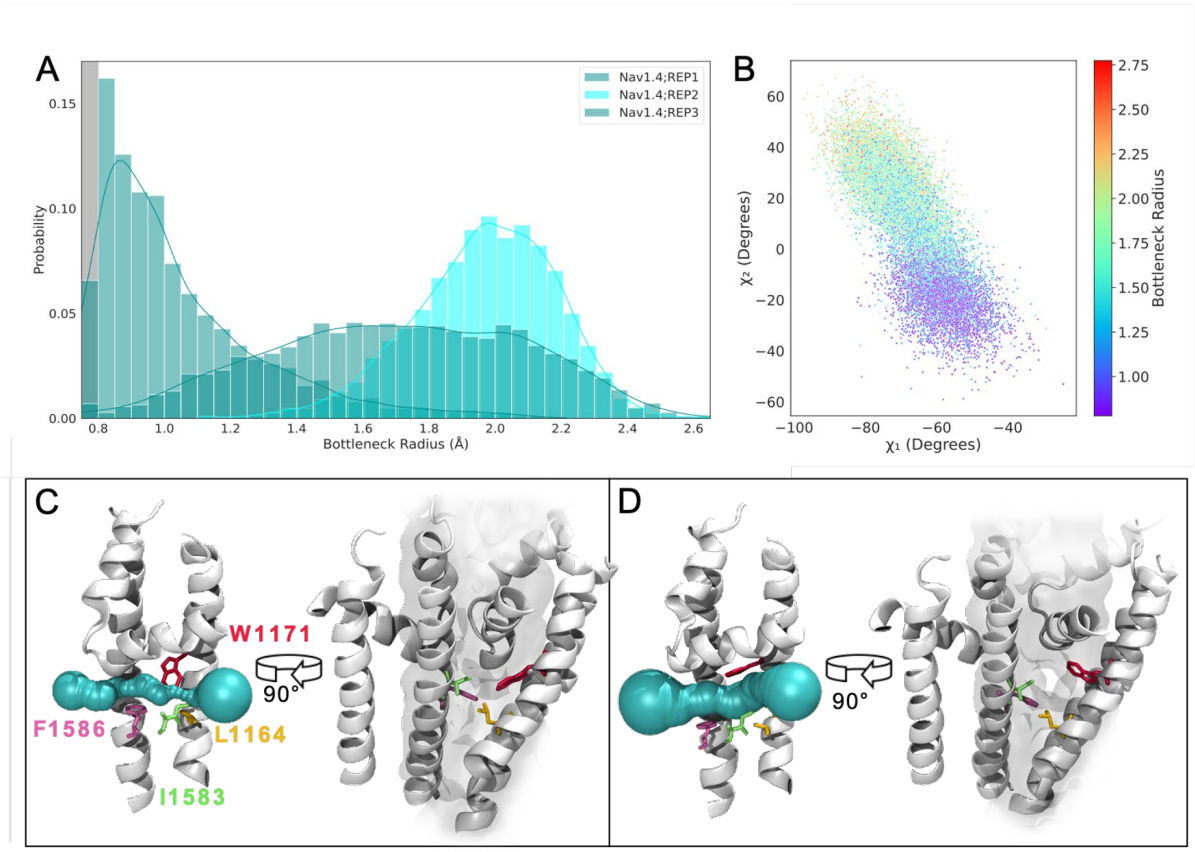

Figure S8 | Bulky S5 residues can also influence fenestration bottleneck radius

Three replicates of Nav1.4 DIII-IV bottleneck radius show highly variable distributions (A). The residue W1171 on DIII-S5 was observed to be highly correlated in its sidechain rotation (both χ1 and χ2 dihedrals) with the size of the bottleneck radius (B). Snapshots are showing the closed (C) and open (D) fenestration appearances, and the positioning of bottleneck residues; the lateral bottleneck created by W1171 on S5 appears to be more significant than the medial bottleneck created by F1586 on S6.

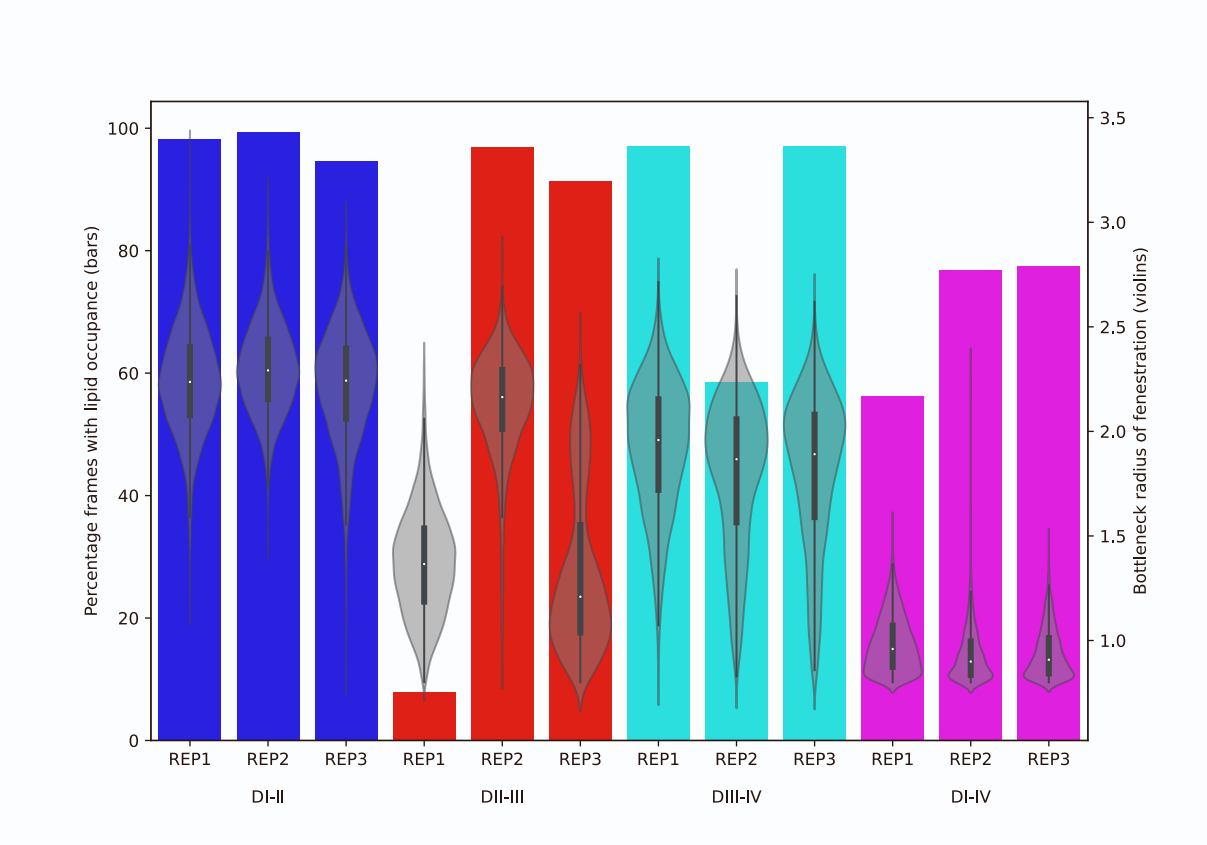

Figure S9 | Comparison between the degree of lipid molecule occupancy in each fenestration and the corresponding fenestration bottleneck radius across the three replicates for hNav1.5.

Lipid tail molecules were detected within a 5 Å cutoff of the S6 position 14/15 bottleneck residue within each fenestration for each frame of the 500 ns simulation replicates. Across most wider fenestration bottlenecks (i.e. DI-II and DIII-IV), there is significant prolonged lipid occupancy throughout simulations. The narrower fenestrations of DII-III and DI-IV show a decreased percentage of frames with lipids present in the fenestrations.

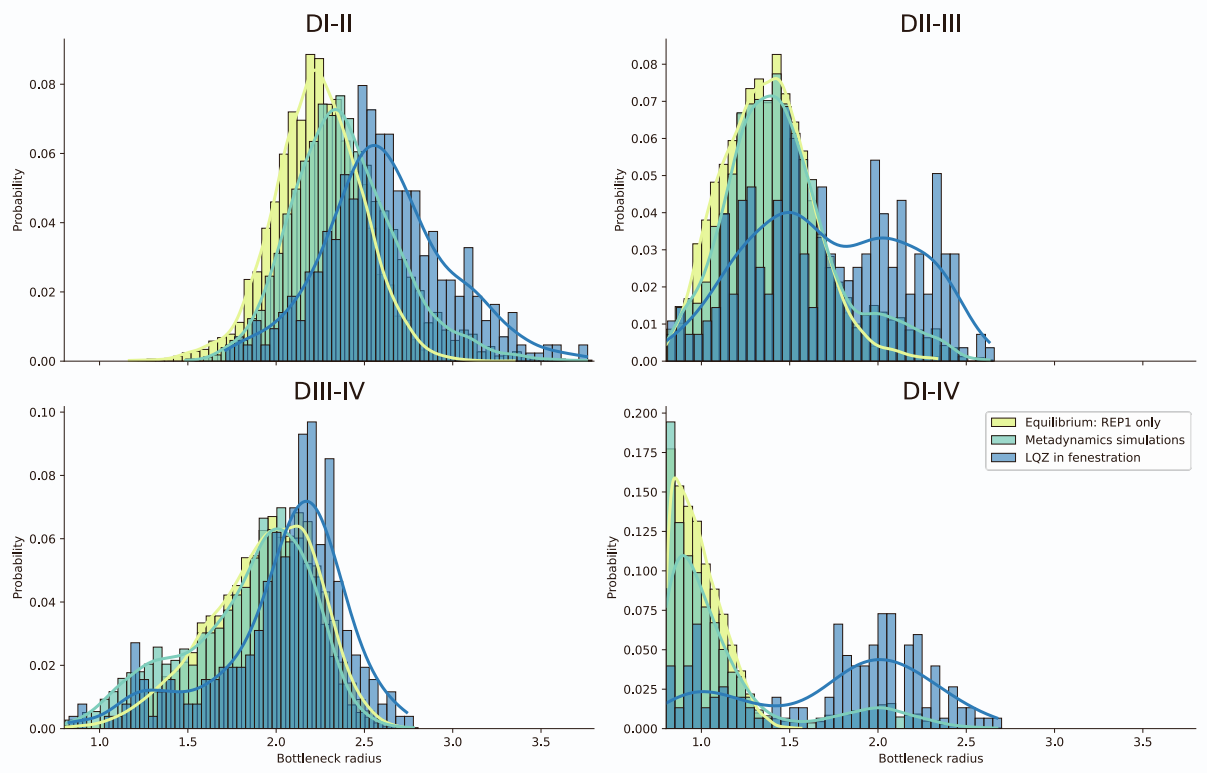

Figure S10 | Effect of lidocaine's (LQZ) presence on the bottleneck radius distributions in Nav1.5 metadynamics simulations.

Bottleneck radius of hNav1.5 throughout metadynamics simulations in the presence of lidocaine (green) show an overall right-shifted distributions compared to the bottleneck distributions in REP1 of hNav1.5 equilibrium simulations (yellow), which suggests noticeable widening of fenestrations. When clustering and selecting for frames where lidocaine was present in each fenestration individually (blue), the widening effect was even more pronounced, highlighting that when lidocaine is located within a fenestration, there is an increased probability of said fenestration adopting a larger bottleneck radius.

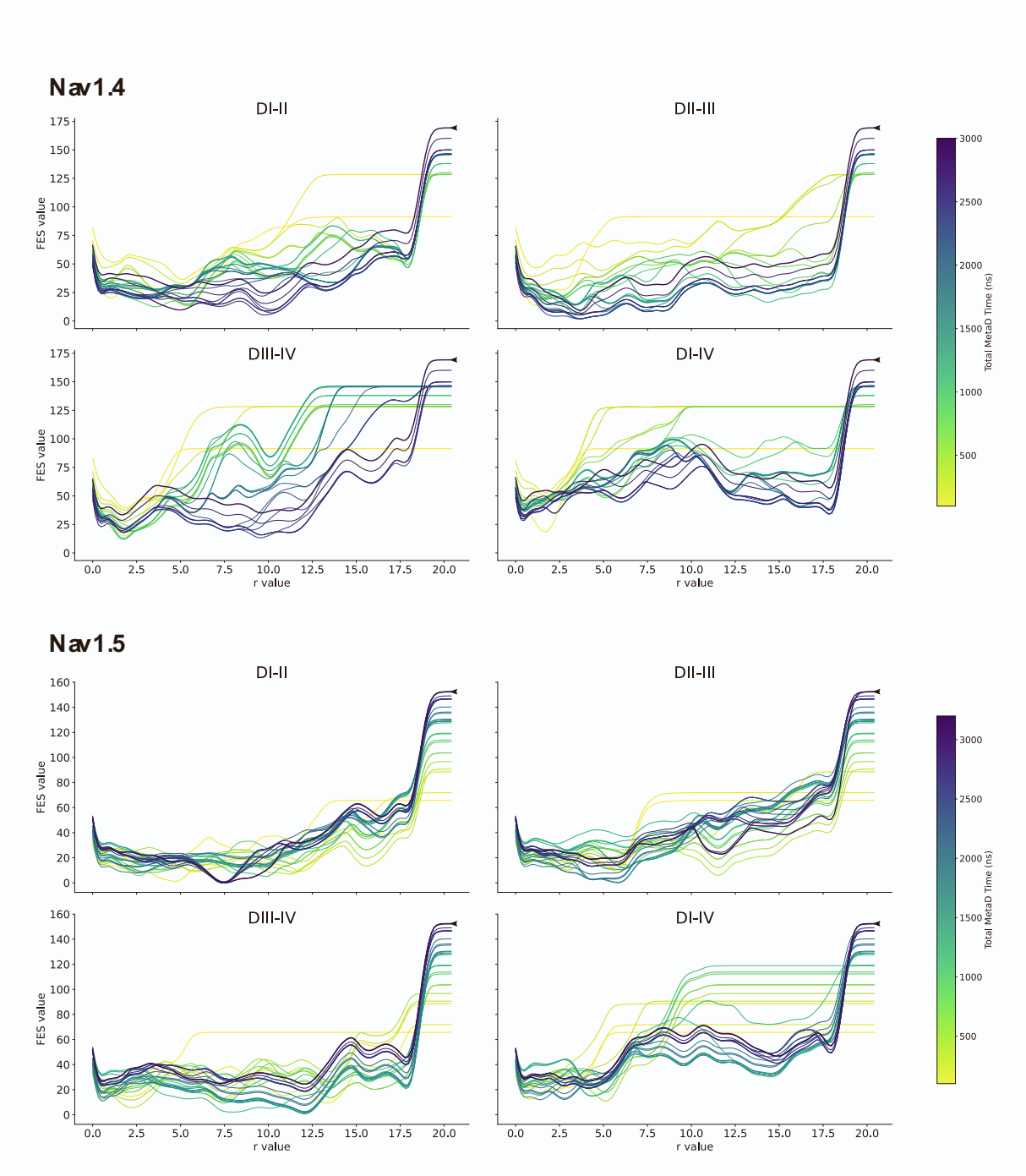

Figure S11 | Convergence of FES from metadynamics simulations.

One-dimensional free energy profiles along the axis of each of the four fenestrations shown for every cumulative 100ns increment of the metadynamics simulations of Nav1.4 (upper four panels) and Nav1.5 (lower four panels). The most recent profile outlined in bold and indicated by the arrow.

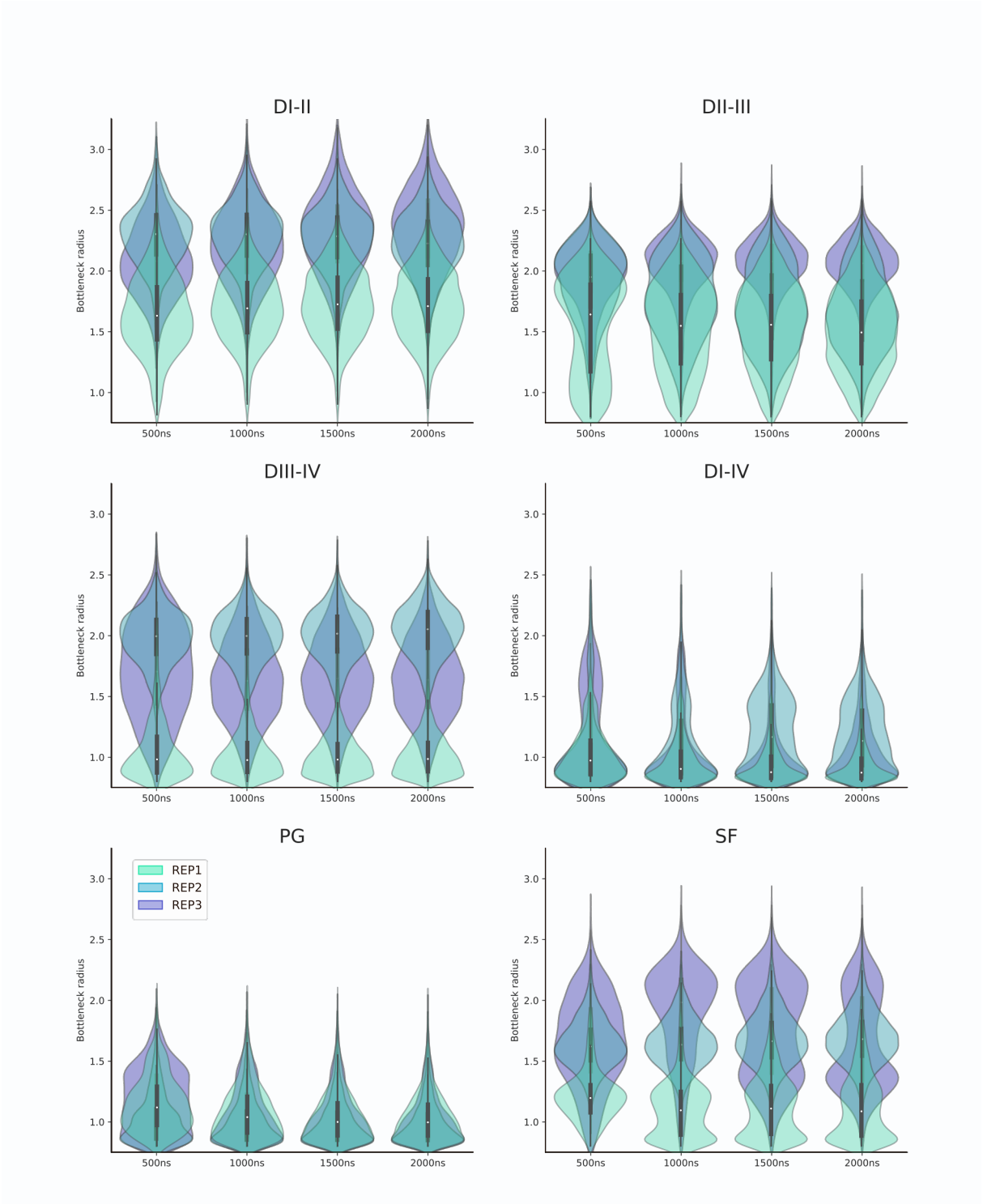

Figure S12 | Assessing convergence of Nav1.4 replicates, after extending equilibrium simulations (to a total of 2 µs).

Bottleneck radius distributions between the replicates, REP1 (cyan), REP2 (blue) and REP3 (purple), remain distinctive when assessed at each 500 ns increment, suggesting convergence is unlikely to be reached in the µs timescale. This suggests that the replicates exist in distinctive conformations and would require significantly longer simulations to converge their structural differences.